

A 100 kW 1.2 kV 20 kHz DC-DC converter prototype based on the Dual Active Bridge topology

Thomas Lagier, Laurent Chédot, François Wallart, Layal Ghossein, Bruno Lefebvre, Piotr Dworakowski, Michel Mermet-Guyennet, Cyril Buttay

▶ **To cite this version:**

Thomas Lagier, Laurent Chédot, François Wallart, Layal Ghossein, Bruno Lefebvre, et al.. A 100 kW 1.2 kV 20 kHz DC-DC converter prototype based on the Dual Active Bridge topology. 2018 IEEE ICIT, Feb 2018, Lyon, France. 10.1109/ICIT.2018.8352238 . hal-01747437

HAL Id: hal-01747437
https://hal.science/hal-01747437

Submitted on 29 Mar 2018

HAL is a multi-disciplinary open access archive for the deposit and dissemination of scientific research documents, whether they are published or not. The documents may come from teaching and research institutions in France or abroad, or from public or private research centers.

L'archive ouverte pluridisciplinaire **HAL**, est destinée au dépôt et à la diffusion de documents scientifiques de niveau recherche, publiés ou non, émanant des établissements d'enseignement et de recherche français ou étrangers, des laboratoires publics ou privés.

A 100 kW 1.2 kV 20 kHz DC-DC converter prototype based on the Dual Active Bridge topology

Thomas Lagier, Laurent Chédot, François Wallart
Layal Ghossein, Bruno Lefebvre, Piotr Dworakowski
Michel Mermet-Guyennet
SuperGrid Institute,
F-69611, Villeurbanne, France

Cyril Buttay

Univ. Lyon, INSA-Lyon, CNRS, Laboratoire Ampère,
UMR 5005
F-69621, Villeurbanne, France

***Abstract*— This article presents the design, the fabrication, and the test of an isolated DC-DC converter for renewable energy applications. The converter is based on the Dual Active Bridge topology and uses silicon carbide power semiconductors and a medium frequency transformer. The design process covers hardware ranging from the semiconductor die to the complete power converter. For the control, a rapid prototyping approach was used. The experimental validation of the 100 kW prototype is presented.**

Keywords*— *DC grids, Medium frequency transformer, Power converters, Renewable energy, Silicon carbide.

I. Introduction

The renewable energy has been expanding over the last decade due to environmental issues. This expansion may even accelerate since the offshore wind power industry becomes profitable without government subsidy [1]. DC distribution networks are proposed to facilitate the interconnection of renewable sources to the electrical grid.

A DC-DC converter is an enabling technology of the DC grid, fulfilling and expanding the role of a transformer in AC grids. Thanks to wide bandgap semiconductors, such as Silicon Carbide (SiC) [2], the power converters can operate at higher voltage and frequency, offering new opportunities for passive components: thanks to this increased switching frequency, the size of the capacitors, inductors and transformers is reduced. Thanks to their lower losses [2], SiC based converters are also expected to be more efficient than those based on silicon devices.

The Dual Active Bridge (DAB) [3], [4] is one of the most promising DC-DC circuit topology for high power applications. The series and/or parallel connection of elementary DABs allows to increase the voltage and power and build converters well suited for medium voltage DC (MVDC) and potentially extensible to high voltage DC (HVDC) applications [5], [6].

This article presents an isolated DC-DC converter that was entirely developed starting from a semiconductor die and finishing with a validation of the complete 100 kW converter. Following the introduction, the second section gives a description of the power converter. The system specification is detailed and the key converter aspects are developed: power electronics, medium frequency transformer and controls. The third section presents the experimental results of the converter prototype. The converter test bench is described and some measurements are presented. The fourth section concludes the paper.

II. DC-DC Converter

A. Specification & topology

The specification of the converter is presented in the TABLE I.

TABLE I. Specification of the converter

Input voltage range (V_{in})	900-1200 V
Output voltage range (V_{out})	450-600 V
Nominal voltage ratio (V_{out}/V_{in})	0,5 ± 10 %
Nominal output power (P_{dc})	100 kW
Switching frequency (f_s)	20 kHz
Cooling system	Air forced

The converter was designed to provide the nominal power over the entire input and output voltage ranges, for an output/input voltage ratio ranging from 0.45 to 0.55. The Dual Active Bridge topology was selected due to its main advantages: power transfer bi-directionality, buck-boost operation, current source behavior and soft switching capability (to reduce the switching losses) [3], [4].

This topology consists of two voltage source inverters linked with an inductive element [3], [4], as depicted in Fig. 1. Several modulation techniques can be implemented with DAB converters [7].

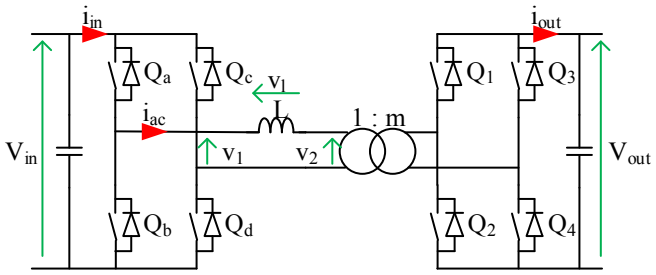


Fig. 1. The Dual Active Bridge topology

Since the nominal voltage range is limited in our case, the converter has been designed considering the phase shifted (or rectangular) modulation. The main advantages of this modulation are: 1) simplicity, 2) losses equally shared between the switches in each inverter, 3) reduced losses when the output/input voltage ratio is close to that of the transformer. Other modulation techniques may be implemented, but with a possible power limitation. The theoretical voltage and current waveforms are presented in Fig. 2.

With the phase shifted modulation, each inverter generates a two-level 50 % duty cycle voltage. The power exchanged is controlled with the phase shift between the two AC voltages (v_1 and v_2):

$$P_{dc} = \frac{kV_{in}^2}{X_l}\Phi\left(1-\frac{\Phi}{\pi}\right) \quad (1)$$

where k is the voltage ratio between the input and output voltage (V_{in} and V_{out}) seen from the primary side of the transformer according to (2), X_l the AC reactance seen from the primary side of the transformer and Φ the phase shift expressed in radians [3].

$$k = \frac{V_{out}}{mV_{in}} \quad (2)$$

where m is the transformer turns ratio.

Regarding the input and output voltage range, it has been decided to use a medium frequency transformer with a turns ratio (m) of 2. It allows the voltage ratio k to be close to 1, so that Zero Voltage Switching (ZVS) is guaranteed over an important range [3]. Moreover, in order to simplify the layout of the converter and to reduce the losses, no external inductance is added and only the leakage inductance of the transformer is considered.

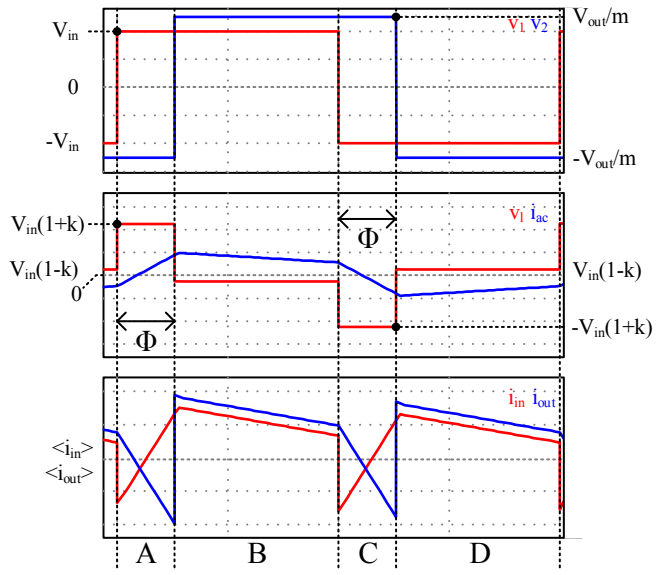


Fig. 2. Thoretical waforms for the phase shifted modulation.

B. *Power electronics*

For the sake of simplicity and of rationality, it was decided to use an identical mechanical layout for the primary and secondary inverters. However, regarding the voltage and current levels (1200 V, 150 A_{RMS} on the primary, 0.6 kV, 300 A_{RMS} on the secondary), different SiC semiconductor devices were used on both sides: 1.7 kV-40 mΩ MOSFET and 1.7 kV-50 A Schottky diode for the primary inverter ; 1.2 kV-25 mΩ MOSFET and 1.2 kV-50 A Schottky diode for the secondary inverter. All devices were supplied by Wolfspeed™ as bare dies [8].

The power modules, integrating a half bridge commutation cell are composed of 5 MOSFET dies and 5 Schottky dies in parallel for each switch. An internal view of the power module is depicted in Fig. 3. Specific power modules were designed for this study, as no suitable SiC module was available on the market at the beginning of the project.

Since the parasitic loop inductance is a key point for fast switching devices, an internal busbar structure was implemented within the power module itself. Moreover, during the soft switching process, the current path commutates from one switch to the opposite diode, so these two elements were placed side by side in the power module. This restricts the change in current path to a very small area, further reducing the parasitic inductance [9]. Finally, as the authors had no experience in connecting a large (5) number of MOSFET dies in parallel, it was decided to provide independent gate and kelvin source terminals for each die in the power module. This complicates the design of the power modules, but makes it possible to separate the gate resistors for each MOSFET die, avoiding any balancing or ringing issue.

Even though they can operate at high temperature [3], unipolar SiC devices offer better efficiency when their junction temperature remains lower than 100 °C. Because of the compact footprint of the power modules (62x108 mm²), heat pipes were inserted in the heatsink to improve thermal spreading. The integration of heat pipes allowed the case temperature of the power module to be reduced by 15 % (for an ambient temperature of 30 °C) as it can been seen in Fig. 4. Finally, the heatsink represents an equivalent thermal resistance of 0.017 °C/W (case to ambient) which allows the junction temperature of the switches to remain lower than 75 °C at the nominal operating point.

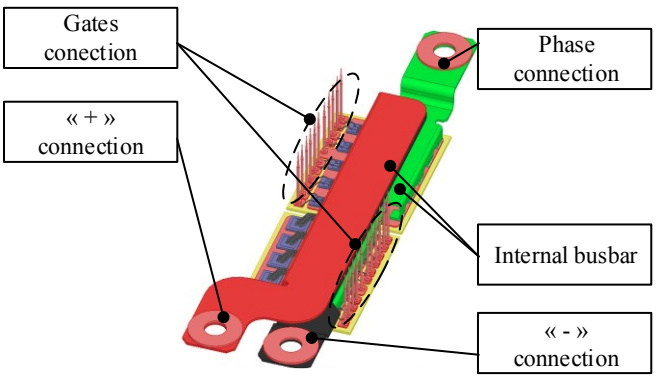
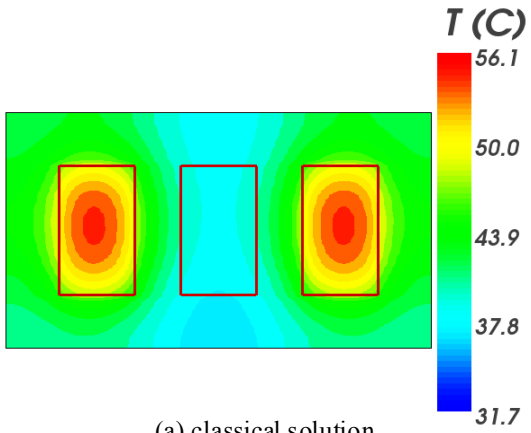
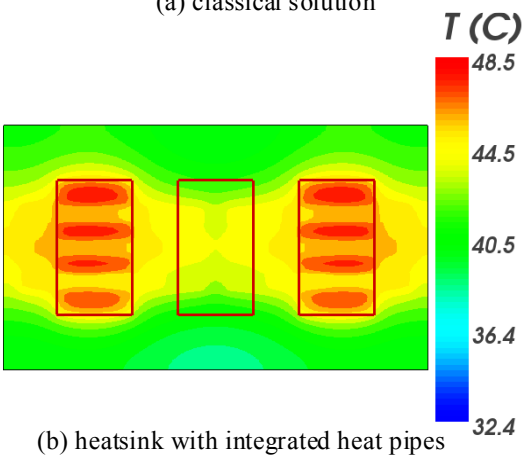


Fig. 3. Internal view of the SiC based power module.



(a) classical solution



(b) heatsink with integrated heat pipes

Fig. 4. Thermal simulations of the heatsink for an ambiant temperature of 30 °C and a dissipated power of 1 kW (500 W for each power module). The results were obtained using R-Tools software [10].

To control the switches, a gate drive board was developed. The gate drive, mainly based on discrete components, is composed of two printed circuit boards as presented in Fig. 5. The distant control board manages the signals and provides the galvanic isolation between the two switches. It is also in charge of the dead times management. The close control board contains the output push-pull stage and the gate resistors. It is located directly against the power module to reduce interconnect length. This board also integrates short-circuit and under-voltage protections.

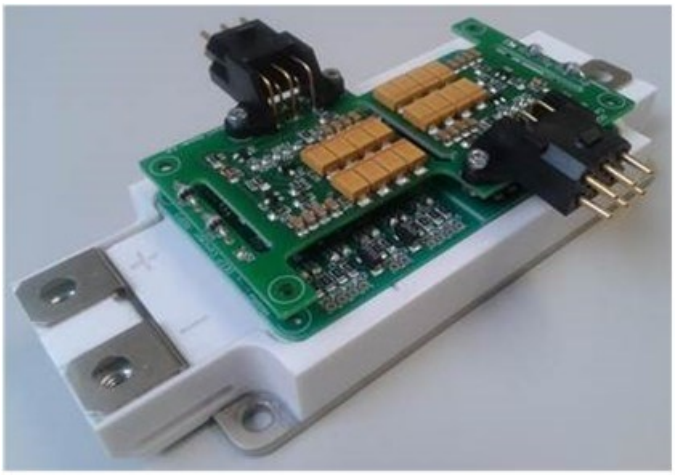
C. Medium Frequency Transformer

1) Main characteristics

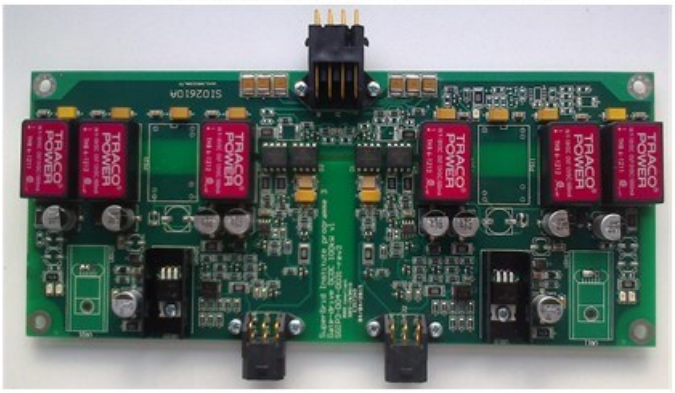
The medium frequency transformer (MFT) was designed according to the requirements of the power converter. The transformer specification is presented in TABLE II.

TABLE II. SPECIFICATION OF THE MEDIUM FREQUENCY TRANSFORMER (MFT)

Apparent power	180 kVA
Primary rated voltage	1200 Vrms
Secondary rated voltage	600 Vrms
Primary rated current	150 Arms
Operating frequency range	17 – 23 kHz
Leakage inductance	As low as possible



(a) Power module (with close control board)



(b) Gate drive (distant control board)

Fig. 5. Power module and gate drive (with close and distant control boards).

Taking into account the additional constraints imposed on the size, weight and volume of the complete device, ferrite was selected as the best magnetic material candidate for the application. Moreover, this material presents lower price and delivery time compared to others. A core-type architecture arranged as a column structure was also seen as the most suitable arrangement of ferrite bars from a manufacturing point of view.

For this application it was essential to calculate the leakage inductance of the transformer with excellent accuracy since this inductance must be kept small (within a few µH), and be well controlled (it directly affects parameter X_l in (1)). As a result, a foil-type winding was selected for both the primary and the secondary windings.

The primary and secondary windings were wound coaxially on each column of the transformer. The primary windings of both columns were connected in series and the secondary windings in parallel. This has the advantage of producing the desired transformation ratio (0.5) on the basis of identical windings.

A metal screen was placed between the primary and secondary windings of each column. It was connected to the metal support of the MFT, itself connected to the ground of the DC-DC converter. The goal was to reduce the parasitic capacitance between the primary and the secondary and to

evacuate the charges to the ground. TABLE III. summarizes the main characteristics of the 180 kVA MFT.

TABLE III. MAIN CHARACTERISTICS OF THE MFT

Structure	Core type, column structure
Magnetic material	Ferrite 3C90, packed in bars
Conductors	Foil on primary, 2 windings of 14 turns in series Foil on secondary, 2 windings of 14 turns in parallel
Volume/Weight	Weight 40kg Vol. 32.5dm^3 Power density 3kW/dm^3

Finally, Fig. 6 presents the final 180 kVA MFT and TABLE IV. gives some electrical measurements and their comparison with the predicted analytic calculation results.

TABLE IV. ELECTRICAL MEASUREMENTS ON THE MFT

	DC		**20 kHz**	
	Measured	**Calculated**	**Measured**	**Calculated**
Primary resistance (mΩ)	4.40	4	10.55	6.25
Secondary resistance (mΩ)	1.02	0.9	2.45	1.41
Leakage inductance (µH)	6	5	6	5

More details on the differences between the measurement and the calculations are given in [11].

1) Thermal measurements

The transformer was equipped with 9 K-type thermocouples to collect a precise temperature map during operation. One thermocouple named "S7", located at the top of the internal magnetic window was representative of the magnetic circuit "hot-spot".

Another one, called "S2", located in the middle of the inner part of the coils, over 2/3 of their height was representative of the windings "hot-spot". A finite element 3D thermal simulation

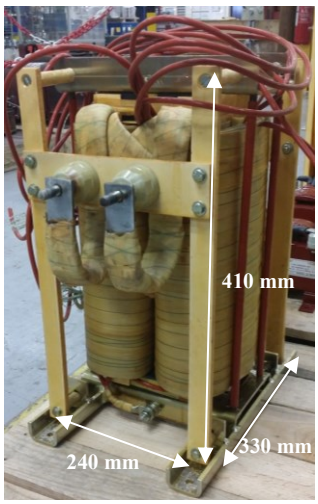


Fig. 6. 180 kVA Medium Frequency Transformer. Thermocouples (red wires) were inserted at various locations of the transformer to monitor the temperature rise in operation.

was carried out using a Computational Fluid Dynamics (CFD) tool (Ansys® ICEpak [12]).

Fig. 7 shows the measured temperatures on "S2" and "S7", in short-circuit condition, for a primary current of 80 Arms at 17 kHz. In those conditions, the "hot-spot" measurements levels were ~ 55 °C on the coils and ~ 40 °C on the magnetic circuit. The measurements were compared with the calculation results including two methods of calculating the copper losses: magnetic 3D on the one hand and analytic (Dowel [13]) on the other hand [11].

III. EXPERIMENTAL RESULTS

A. Converter layout

The electrical diagram and the picture of the DC-DC converter prototype are presented in Fig. 8. Since the DAB topology can be implemented in single-phase or three-phase configurations, the prototype was designed so it can host three-leg inverters. However, for this first version, only a single-phase topology was implemented and the third leg is used as a crowbar switch for protection purpose.

Several sensors were implemented in the converter for control and protections aspects. Moreover, each inverter integrates a bleeding resistor which ensures the slow discharge of the capacitors (a few minutes) for safety purpose.

From Fig. 8b, it should be noted that the power density of the converter was not the main design criterion. For example large heatsinks and driver boards were used, which could have been made sensibly more compact. As it is, the power density of the converter is around 0.71 kW/dm^3.

Finite elements (Ansys® Q3D Extractor and Simplorer [12]) and time-domain simulations were used to estimate the global parasitic inductance of the commutation loop (from the capacitors to the dies). Then, a double-pulse test was performed to validate the simulation models. Consequently, the global parasitic inductance was estimated to be 70 nH. This value is acceptable considering the switching rise time and the soft switching operation of the converter.

B. Control system

The control system manages the operation of the test bench (power supply, auxiliaries) and controls the converter(s). The design flow for the control system is based on Rapid Control Prototyping (RCP) using a Speedgoat™ real-time controller [14] which hosts a CPU and a FPGA.

The control algorithms were designed and tested in a simulation environment using Matlab/Simulink® with the particular use of Simscape Power Systems to simulate the test bench and the DAB(s). Once the control satisfied the requirements, the code was automatically generated for both the CPU and the FPGA using Mathworks® Coders (Maltab/Simulink coder and HDL coder), downloaded on the real-time target machine ready for testing on the real system.

The HMI (Human Machine interface) realized with Simulink Real-time Explorer allowed to set the voltage and power references of the DABs as well as to monitor the system.

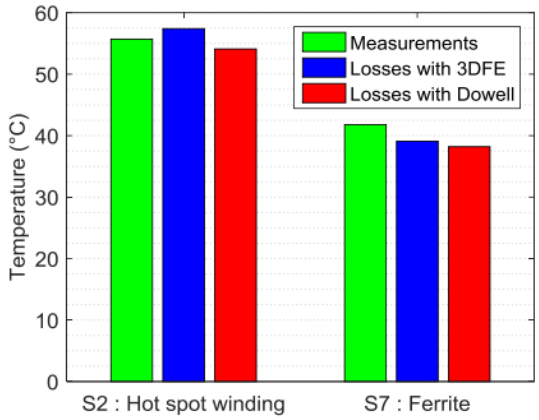
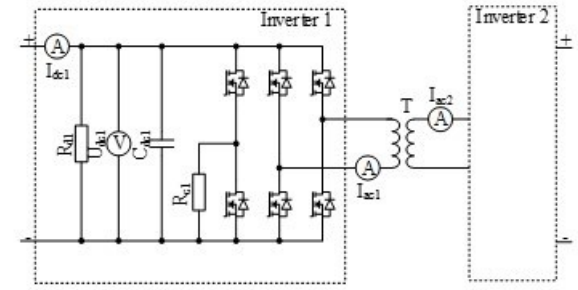
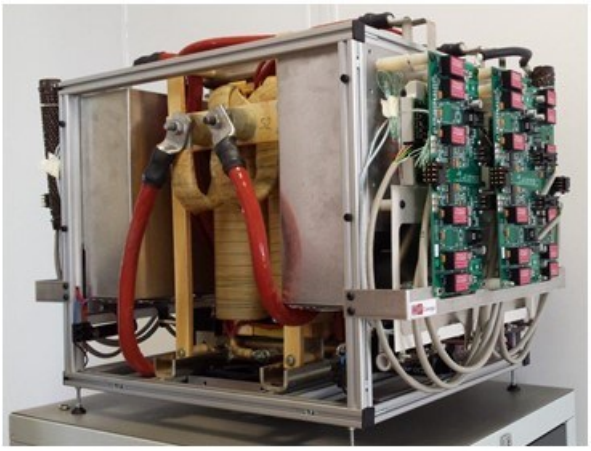


Fig. 7. Thermal measurements for an ambiant temperature of 20 °C.



(a) diagram of the DC-DC converter



(b) picture of the DC-DC converter

Fig. 8. Circuit diagram and picture of the DC-DC converter prototype

The real-time controller was a Speedgoat™ Performance Target Machine featuring a 3.5GHz core i7 CPU, a digital 24V I/O board (IO204) and a programmable FPGA module (Spartan 6 150k) with fast analog and digital I/O (IO331-06-21). The architecture of the control can be observed in the integration model in Fig. 9.

It is noteworthy that a variant model was used for FPGA and CVS&BENCH subsystems. Upon the value of a configuration parameter, the FPGA model was either a simplified version, a complete version used to generate the bitstream (@20ns) or the bitsteam itself. A variant model was also used for the converter and the test bench (CVS&BENCH).

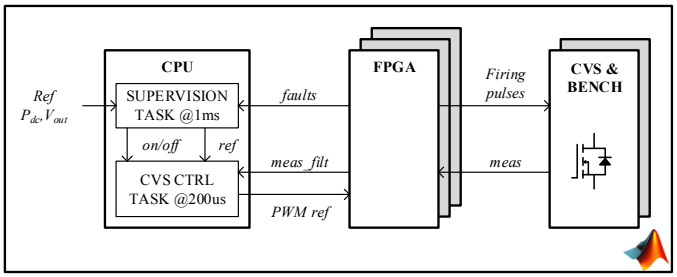
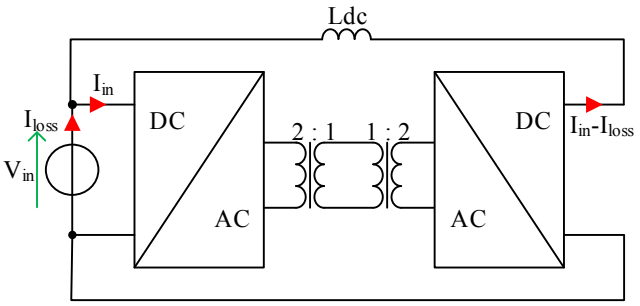


Fig. 9. Architecture of the integration model in Simulink

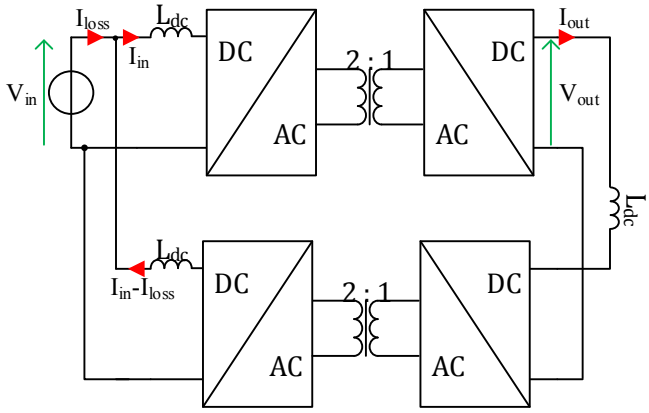
In simulation, the system was modeled with Simscape Power Systems and for code generation, the variant model points to an empty subsystem.

C. Test bench

The converter was tested using two configurations as depicted in Fig. 10. In the first configuration (Single standalone converter), two MFT are cascaded so that the equivalent turns ratio equals one, allowing the connection of the converter input to the output. For this configuration, each inverter is equipped with 1.7 kV SiC MOSFET power modules. In the second configuration (Back to back converters), two DC-DC converters are cascaded with an intermediate DC bus. One converter controls the voltage of the low voltage bus (V_{out}) while the other controls the current (I_{out}). Those two configurations allow the converter to be tested under the nominal voltage and power (100 kW) but only requires a low power supply (4-5 kW). DC inductors (L_{dc}) were used in the DC buses for decoupling.



(a) Single standelone converter



(b) Back to back converters

Fig. 10. Two configurations used for the testing of the converter.

D. Measurements

Fig. 11 presents the experimental waveforms, where v_{ac1} and v_{ac2} are the output voltage of the inverters and i_{ac} the current on the primary side of the transformer. At this operating point, the RMS value of the AC current is about 100 A. The phase shift between the two AC voltages is 13 ° at 20 kHz.

Two approaches have been used to estimate the efficiency of the converter. The first one is based on the power delivered by the DC supply where the losses of the DC inductors are subtracted (requiring an accurate characterization of the inductors). The second one is based on the input and output current and voltage measurements. In order to improve the accuracy, the complete acquisition chain was calibrated.

The efficiency estimation was performed for the single standalone converter configuration. In this case, the losses are generated by two inverters and two transformers. Fig. 12 presents the efficiency estimation for the input voltage of 1 kV. For the transmitted power of 100 kW, the estimated efficiency is around 97.3 %.

Regarding this result, the authors expect that 98% efficiency may be achieved with one transformer at the nominal voltage 1.2 kV. Other measurements are in progress in the back to back converters configuration in order to validate this point.

IV. Conclusion

This article presents a unique development, ranging from the semiconductor die to the complete converter. This offered a lot of flexibility in the design. A test system, based on rapid control prototyping, proves that the converter performance fulfills the requirements specification.

The combination of silicon carbide, medium frequency transformer and Dual Active Bridge technologies exhibit very promising performance. However, the remaining challenge is the management of the electromagnetic interferences, which were not addressed early enough in our design and proved difficult to contain. The extension of the technology to medium or high voltage applications requires significant efforts in the insulation coordination. The three-phase DAB seems to be an interesting configuration for the very high power applications and will be further analyzed by the authors.

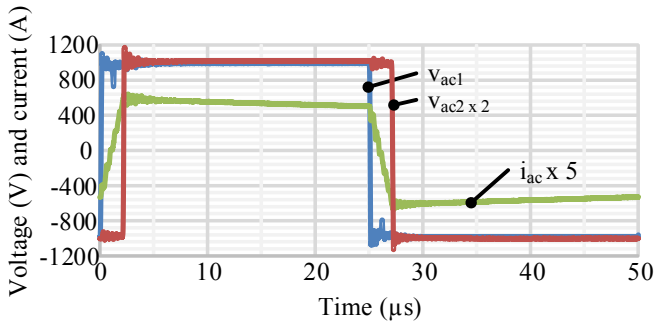


Fig. 11. Waveforms of one DAB converter (V = 1 kV ; k = 1 ; P_{dc} = 100 kW).

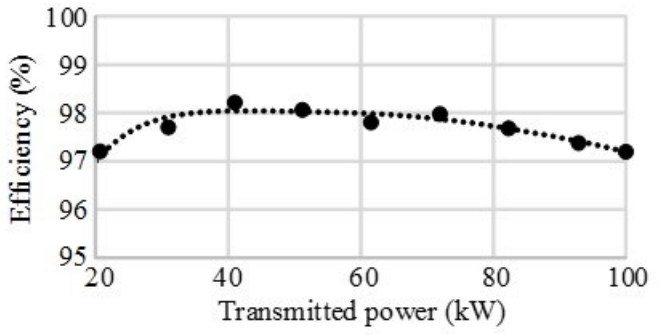


Fig. 12. Efficiency estimation for the standelone (two inverters + two transformers) configuration for the input voltage of 1 kV.

V. Acknowledgment

This work was supported by a grant overseen by the French National Research Agency (ANR) as part of the "Investissements d'Avenir" Program (ANE-ITE-002-01).

The authors would like to thank TRANSRAIL B&V, DEEP Concept and Plateforme Primes for their support with the development of the converter prototype.

VI. References

[1] P. Fairley, "For the first time, offshore wind power will be profitable without subsidies.," *IEEE Spectrum*.

[2] J. Millán, P. Godignon, X. Perpiñà, A. Pérez-Tomás, and J. Rebollo, "A Survey of Wide Bandgap Power Semiconductor Devices," *IEEE Transactions on Power Electronics*, vol. 29, no. 5, pp. 2155–2163, May 2014.

[3] M. N. Kheraluwala, R. W. Gascoigne, D. M. Divan, and E. D. Baumann, "Performance characterization of a high-power dual active bridge DC-to-DC converter," *Industry Applications, IEEE Transactions on*, vol. 28, no. 6, pp. 1294–1301, Nov. 1992.

[4] R. W. De Doncker, M. H. Kheraluwala, and D. M. Divan, "Power conversion apparatus for DC/DC conversion using dual active bridges," 1991.

[5] T. Lagier and P. Ladoux, "A comparison of insulated DC-DC converters for HVDC off-shore wind farms," in *2015 International Conference on Clean Electrical Power (ICCEP)*, 2015, pp. 33–39.

[6] T. Lagier, P. Ladoux, and P. Dworakowski, "Potential of silicon carbide MOSFETs in the DC/DC converters for future HVDC offshore wind farms," *High Voltage*, Jul. 2017.

[7] N. Schibli, "Symmetrical multilevel converters with two quadrants DC-DC feeding," Ecole Polytechnique Federale de Lausanne, 2000.

[8] *WolfSpeed (2017, October.),Wolfspeed Power Products [Online]. Avaible: http://www.wolfspeed.com/power/products*. .

[9] Z. Chen, Y. Yao, W. Zhang, D. Boroyevich, K. Ngo, P. Mattavelli, and R. Burgos, "Development of a 1200 V, 120 A SiC MOSFET module for high-temperature and high-frequency applications," in *The 1st IEEE Workshop on Wide Bandgap Power Devices and Applications*, 2013, pp. 52–59.

[10] *Mersen (2017, October.),R-Tools [Online]. Avaible: http://ep-us.mersen.com/solutions/cooling-of-power-electronics/r-tools2/*. .

[11] A. Pereira, F. Sixdenier, M. A. Raulet, B. Lefebvre, and N. Burais, "Comparison Between Numerical and Analytical Methods of AC Resistance Evaluation for Medium-Frequency Transformers: Validation on a Prototype and Thermal Impact Analysis," *Canadian Journal of Electrical and Computer Engineering*, vol. 40, no. 2, pp. 101–109, 2017.

[12] *Ansys (2017, October.), Electromagnetic simulation products [Online]. Avaible: http://www.ansys.com/products/electronics*. .

[13] P. L. Dowell, "Effects of eddy currents in transformer windings," *Electrical Engineers, Proceedings of the Institution of*, vol. 113, no. 8, pp. 1387–1394, Aug. 1966.

[14] *Speedgoat (2017, October.), Speedgoat - Simulink x86 and FPGA real time target [Online]. Avaible: https://www.speedgoat.com*. .